Supplement of

Contrasting air pollution and surface temperature trends in South and East Asia: satellite observations and CMIP6 simulations assessment

Selviga Sinnathamby et al.

Correspondence to: Selviga Sinnathamby (selviga.sinnathamby@latmos.ipsl.fr)

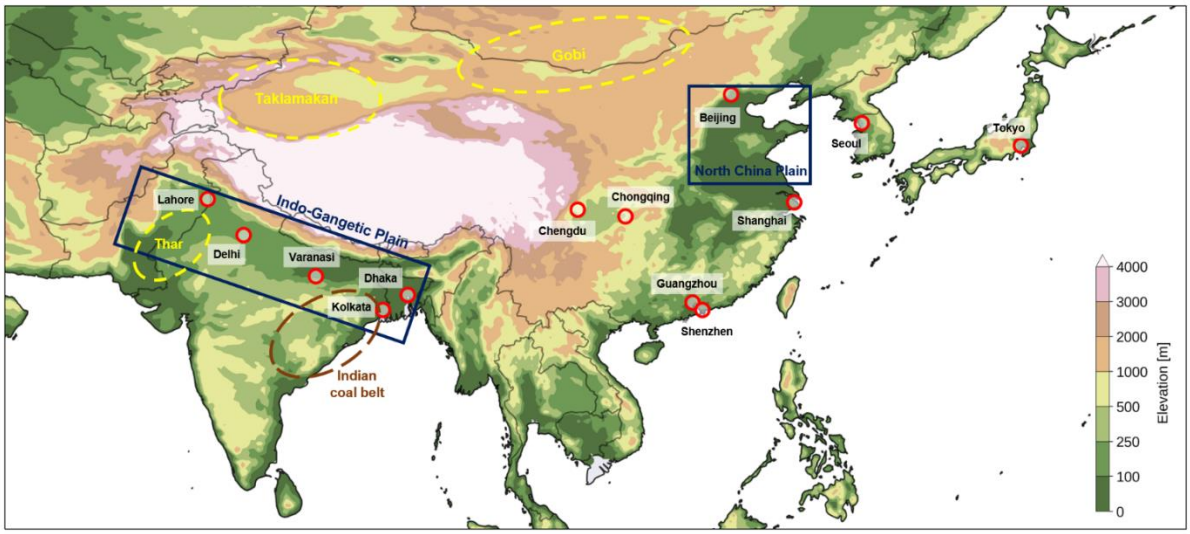

Figure S1. Elevation map of South and East Asia showing the locations of the discussed cities and sub-regions, including the Indo-Gangetic Plain, the North China Plain, the Indian Coal Belt, and regional deserts. Note that the boundaries shown for the sub-regions are approximate.

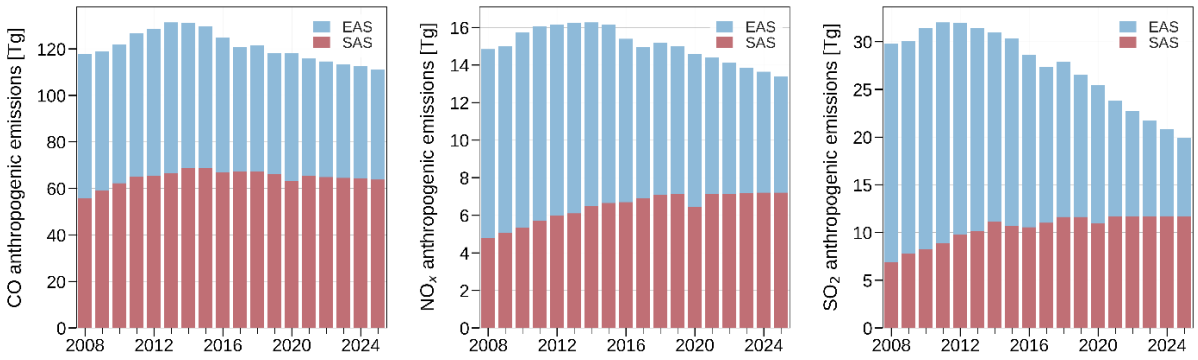

Figure S2. Yearly anthropogenic emissions of CO, NO_x and SO_2 in East Asia (EAS, in blue) and South Asia (SAS, in pink), as given by the CAMS-GLOB-ANTv6.2 inventory. In East Asia, CO, NO_x and SO_2 anthropogenic emissions underwent a decline of -6%, -10% and -33% by 2025 relative to 2008, respectively. Rather than a steady linear decrease, the decline strictly began around 2013, aligning with the implementation of the APPCAP in China. In contrast, South Asia experienced an overall increase in emissions over the 2008-2025 period (+14% for CO, +50% for NO_x, and +70% for SO_2) but these evolutions were not strictly monotonic. CO emissions rose until 2015 (+23% relative to 2008) before entering a phase of gradual decline (-7% relative to 2015).

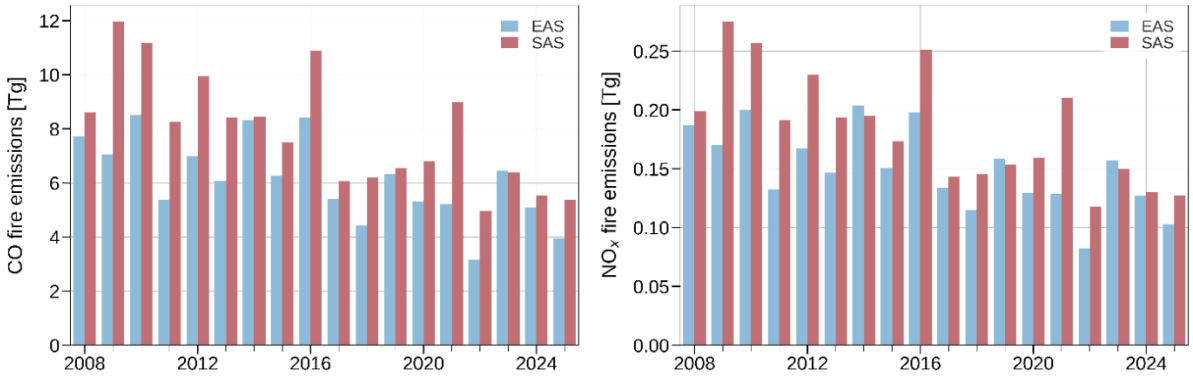

Figure S3. Yearly fire emissions of CO and NO_x in East Asia (EAS, in blue) and South Asia (SAS, in pink), as given by the GFASv1.2 inventory. Both South and East Asia show a steady decline in CO and NO_x emissions from biomass burning, with changes in 2025 relative to 2008 of -48% and -46% for South Asia, and -37% and -39% for East Asia, respectively.

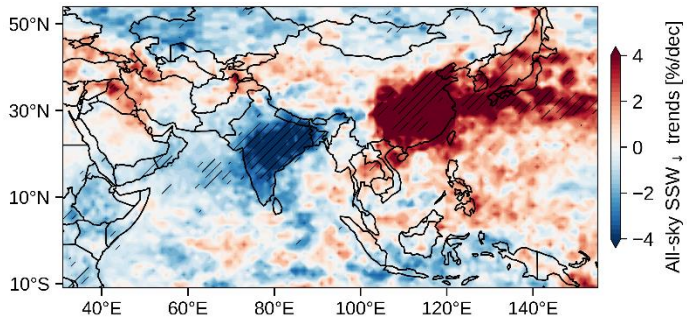

Figure S4. All-sky SSW↓ trends over the 2008-2025 period, as provided by the CERES EBAF dataset. Significant trends are hatched. We find significant trend values of -2.4 ± 0.7 and +3.5 ± 0.9 %/dec in South Asia and East Asia, respectively.

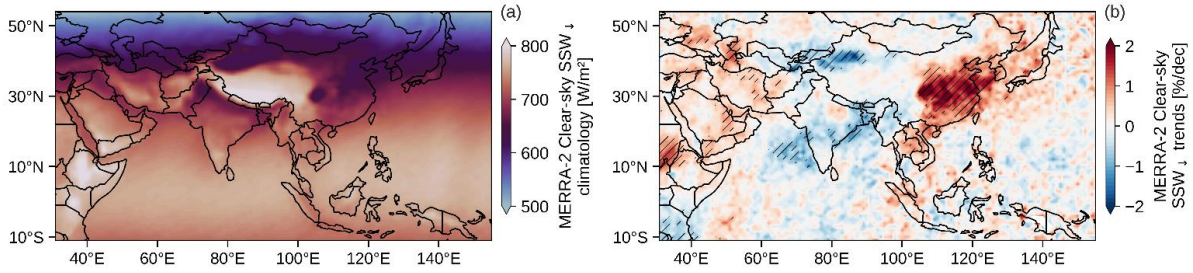

Figure S5. Spatial distribution of MERRA-2 clear-sky SSW↓ (a) and associated trends (b) over the 2008-2025. MERRA-2 clear-sky SSW↓ was beforehand spatially and temporally matched to IASI clear-sky daytime overpass. Significant trends are hatched. We find a non-significant trend of -0.2 ± 0.2 %/dec in South Asia and a significant positive trend of +0.9 ± 0.4 %/dec in East Asia.

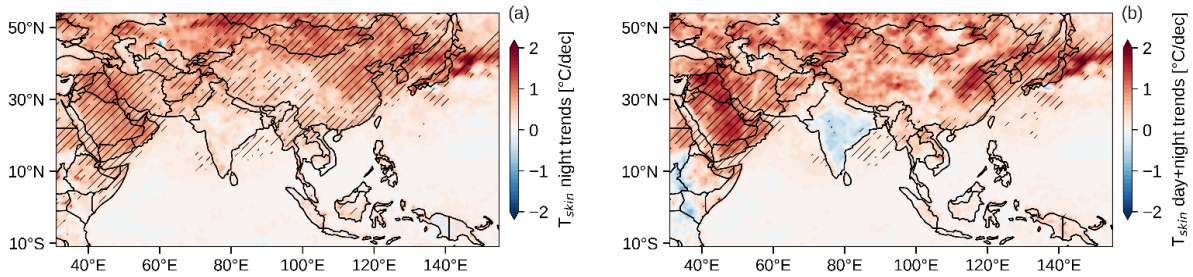

Figure S6. IASI T_{skin} trends over 2008-2025 for nighttime observations (a) and combined daytime and nighttime observations (b). Significant trends are hatched.

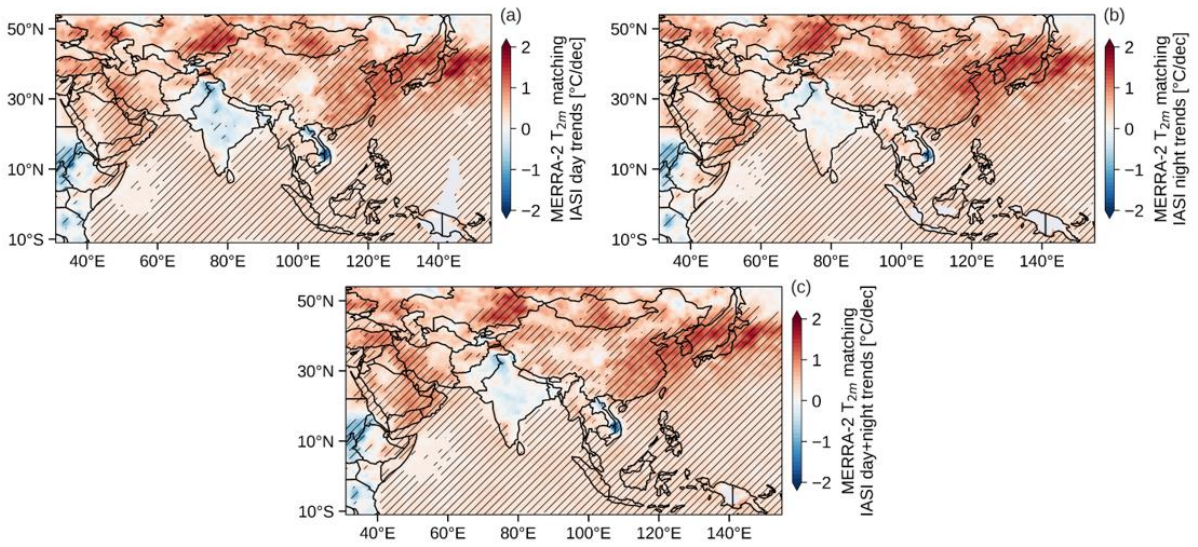

Figure S7. Trends in MERRA-2 air temperature at 2-meter (T_{2m}) spatially and temporally matched to IASI daytime (a), nighttime (b), and combined daytime and nighttime (c) overpasses over 2008-2025. Significant trends are hatched. For daytime observations, we find T_{2m} trend values on average over land of -0.1 ± 0.8 °C/dec in South Asia and +0.7 ± 0.9 °C/dec in East Asia. At nighttime, trends values are +0.1 ± 0.7 °C/dec in South Asia and +0.8 ± 0.8 °C/dec in East Asia. For the combined daytime and nighttime T_{2m} trends, we find values of -0.1 ± 0.7 °C/dec in South Asia and +0.7 ± 0.1 °C/dec in East Asia. All trends in East Asia are statistically significant.

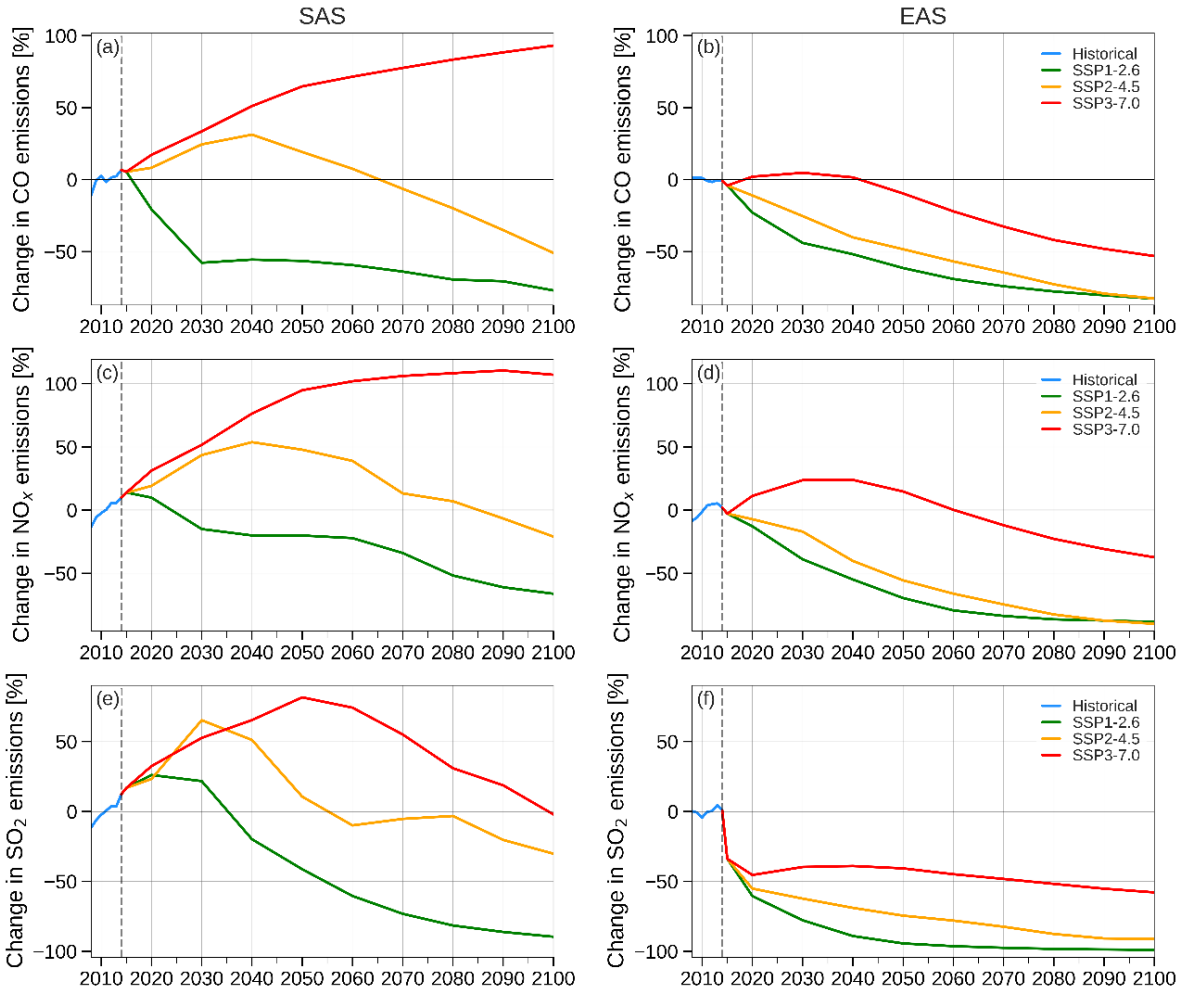

Figure S8. Relative changes of CMIP6 emissions (anthropogenic and biomass burning combined) of CO, NO_x and SO_2 in South Asia (SAS, left column) and East Asia (EAS, right column) over the 2008-2100 period. Changes are calculated relative to the 2008-2014 average emission levels. Results are shown for the historical simulation (blue), SSP1-2.6

(green), SSP2-4.5 (yellow) and SSP3-7.0 (red). The vertical dotted line at 2014 in each subplot marks the transition from the historical simulation to the SSPs.

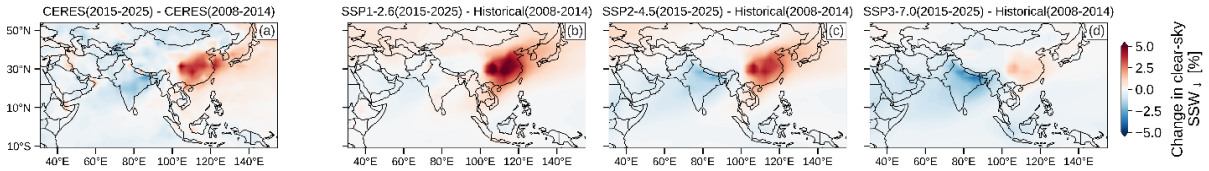

Figure S9. Relative changes (2015-2025 vs. 2008-2014) in clear-sky SSW↓ as observed by CERES (a) and as simulated in the CMIP6 multi-model mean under SSP1-2.6 (b), SSP2-4.5 (c), and SSP3-7.0 (d).

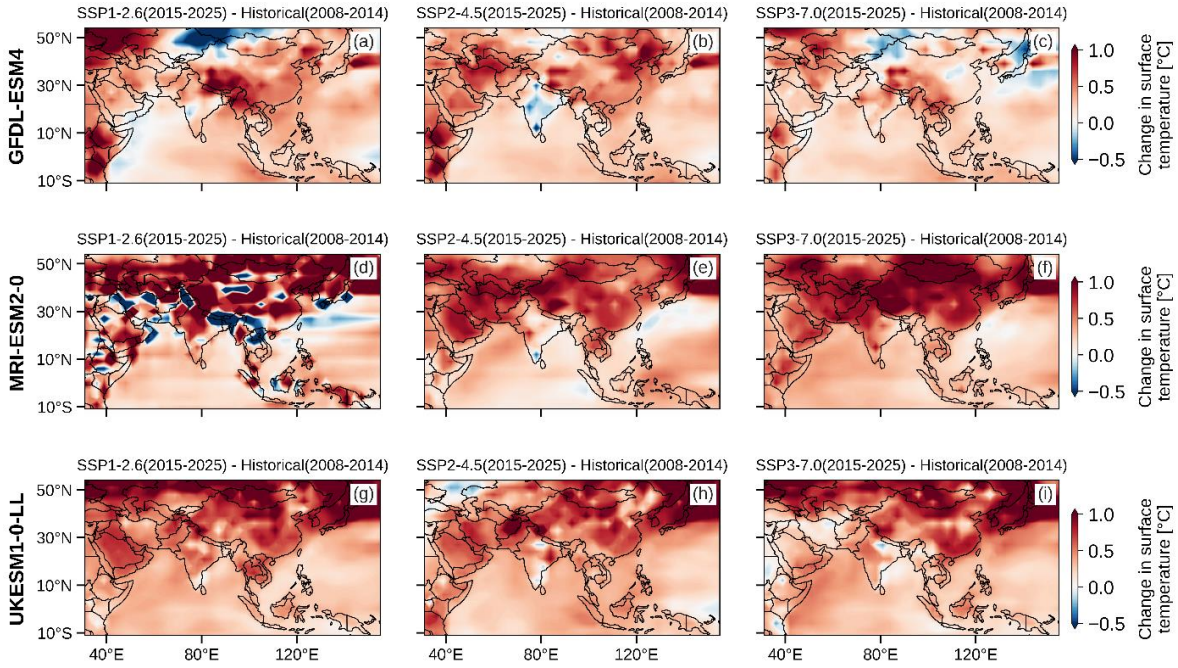

Figure S10. Simulated relative changes (2015-2025 vs. 2008-2014) in surface temperature (top to bottom) from GFDL-ESM4, MRI-ESM-0 and UKESM1-0-LL models, under SSP1-2.6 (first column), SSP2-4.5 (second column), and SSP3-7.0 (third column).

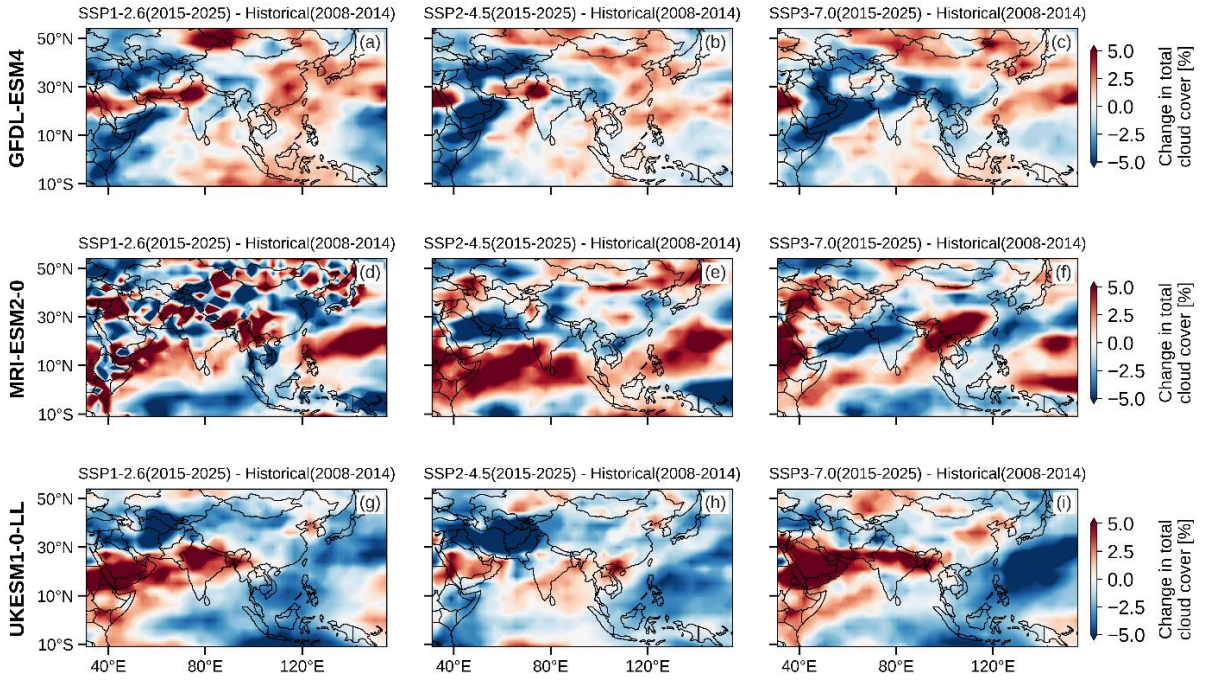

Figure S11. Simulated relative changes (2015-2025 vs. 2008-2014) in total cloud cover (top to bottom) from GFDL-

ESM4, MRI-ESM-0 and UKESM1-0-LL models, under SSP1-2.6 (first column), SSP2-4.5 (second column), and SSP3-7.0 (third column).

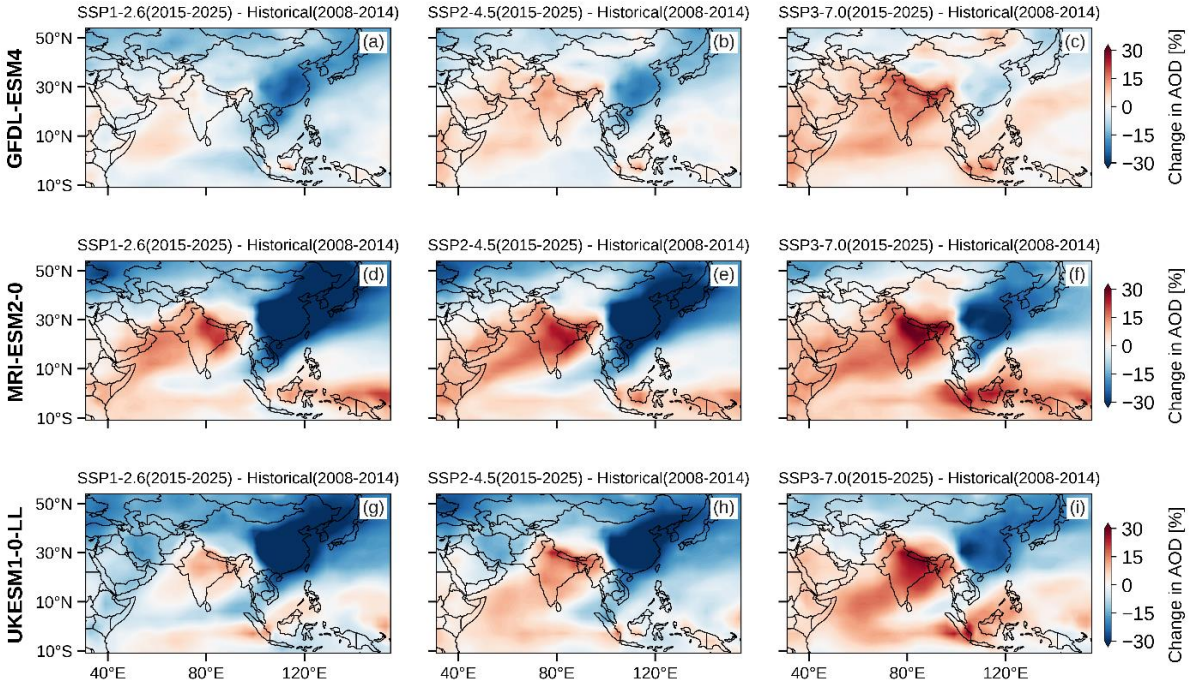

Figure S12. Simulated relative changes (2015-2025 vs. 2008-2014) in AOD (top to bottom) from GFDL-ESM4, MRI-ESM-0 and UKESM1-0-LL models, under SSP1-2.6 (first column), SSP2-4.5 (second column), and SSP3-7.0 (third column).